

Lithologic mapping in arid regions with Landsat thematic mapper data: Meatiq dome, Egypt

MOHAMED SULTAN } McDonnell Center for the Space Sciences, Department of Earth and Planetary Sciences, Washington University,
RAYMOND E. ARVIDSON } St. Louis, Missouri 63130
NEIL C. STURCHIO } Argonne National Laboratory, Argonne, Illinois 60439
EDWARD A. GUINNESS } McDonnell Center for the Space Sciences, Department of Earth and Planetary Sciences, Washington University,
St. Louis, Missouri 63130

ABSTRACT

Digital Landsat thematic mapper (TM) data were evaluated for lithologic mapping capabilities over the Meatiq dome area in the hyper-arid Eastern Desert of Egypt. Bi-directional spectral reflectance data (0.4–2.5 μm) for powders of the major rock types exposed in the dome and published spectral reflectance data were used as guides in selecting TM band reflectance ratios that maximize discrimination of individual rock types on the basis of their respective mineralogies. Comparison of TM data with field and petrographic observations shows (1) increasing amounts of magnetite and other opaque minerals, with low, flat spectral reflectances, decrease the ratio of TM band 5 (1.55 to 1.75) to band 1 (0.45 to 0.52 μm); (2) increasing amounts of hydroxyl-bearing minerals, with hydroxyl ion vibrational absorptions in TM band-7 wavelength region (2.08 to 2.35 μm), increase the ratio of TM band 5 to band 7; (3) increasing amounts of Fe-bearing aluminosilicates that absorb in the band-4 wavelength region (0.76 to 0.9 μm) increase the product of the following two TM ratios: band 5 to band 4 and band 3 (0.63 to 0.69 μm) to band 4; and (4) thin ($\leq 5 \mu\text{m}$), desert varnish that covers many outcrops modulates, but does not obscure, the spectral reflectance signatures of the Meatiq rocks. The varnish consists of amorphous to poorly crystalline dioctahedral smectite, iron oxides, and/or oxyhydroxides. Serpentine, mafic mylonite, massive amphibolite, quartzofeldspathic mylonite, biotite schist, and quartz phyllonite were mapped on the basis of their unique values in one or more of the three ratio images, whereas coarse- and fine-grained granites, granite gneiss, and tonalite, with similar mineralogies and TM band ratios, were mapped as a group. Finer subdivisions were made where field traverses provided local verification. Results demonstrate that appropriate processing and presentation of Landsat TM data can significantly augment field observations for lithologic mapping of large areas in arid regions.

INTRODUCTION

Remote sensing observations provide coverage of large areas with quantitative observational parameters (for example, spectral radiance or power received in case of thematic mapper [TM] data) and are thus a potentially rich source of information for lithologic mapping. A scene acquired by the Landsat TM instrument covers 185 by 185 km, with seven broad spectral bands (Engel and Weinstein, 1982). Six of the bands detect

reflected visible and infrared radiation (0.45 to 2.35 μm) and have image-element widths 30 by 30 m.

The primary objective of this paper is to demonstrate that valuable and systematic mineralogical inferences can be made from TM data covering arid terranes. The techniques advocated are straightforward and are based on the identification of spectral reflectance features common to many rock types. The Meatiq dome (Fig. 1) was chosen as a test site to explore TM processing and presentation techniques for the following reasons. (1) A diverse suite of igneous and metamorphic rocks is exposed. The rock types include many of the late Proterozoic crystalline rock units

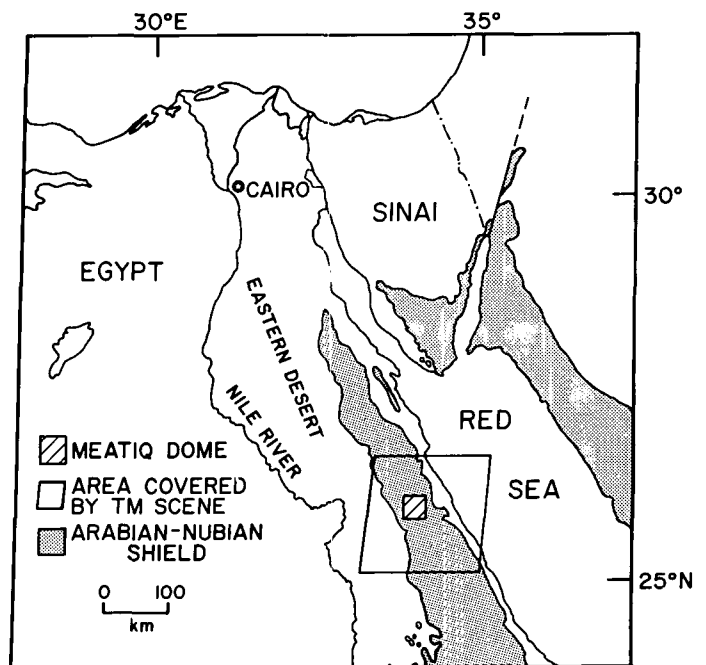


Figure 1. Place map showing location of study area in the Eastern Desert, Egypt. The shaded areas mark outcrops of the late Proterozoic rocks that are parts of the Arabian-Nubian Shield. The TM scene used: ID 5015707420, path 174, row 42, center lat. 26.01°N, center long. 33.81°E, date acquired 8/05/84, sun elevation 58° above horizon, and sun azimuth 94° clockwise from north.

of the Eastern Desert of Egypt and the Arabian-Nubian Shield. (2) The authors have conducted detailed field, petrographic, and geochemical studies in the area (Sturchio and others, 1983, 1984; Sturchio and Muehlenbachs, 1985; Sultan, 1984; Sultan and others, 1986c). (3) Vegetation and soil cover that might strongly modulate rock spectral reflectance signatures are virtually absent due to the hyper-arid conditions. In addition, detailed mapping on a regional basis has not yet been accomplished for much of the Arabian-Nubian Shield. Thus, augmentation of our understanding of the outcrop distribution of major rock types in the Meatiq area can serve as a starting point for construction of TM-derived lithologic maps over wider regions of the Shield.

The paper is organized in the following manner. First, mineralogical controls on spectral reflectance data for the dominant rock types exposed in the dome area are discussed. The extent to which the ubiquitous desert varnish obscures the reflectance signatures of underlying rocks is then

explored. TM data are then discussed, stressing processing and presentation procedures that emphasize the dominant mineralogical controls for Meatiq rocks, while minimizing spectral variations due to topography and to grain size differences. The use of resultant image products in the compilation of a new lithologic map is then discussed. Finally, results specific for the Meatiq area are summarized, and general implications are drawn with regard to both capabilities and limitations associated with TM-based lithologic mapping in arid regions.

GEOLOGY OF THE MEATIQ DOME

The Meatiq dome is a doubly plunging, open antiformal structure (Fig. 2) consisting of a conformable sequence of amphibolite-grade metamorphic units (Sturchio and others, 1983). In ascending structural order, the main lithologic units are (1) granite gneiss; (2) quartzofeldspathic

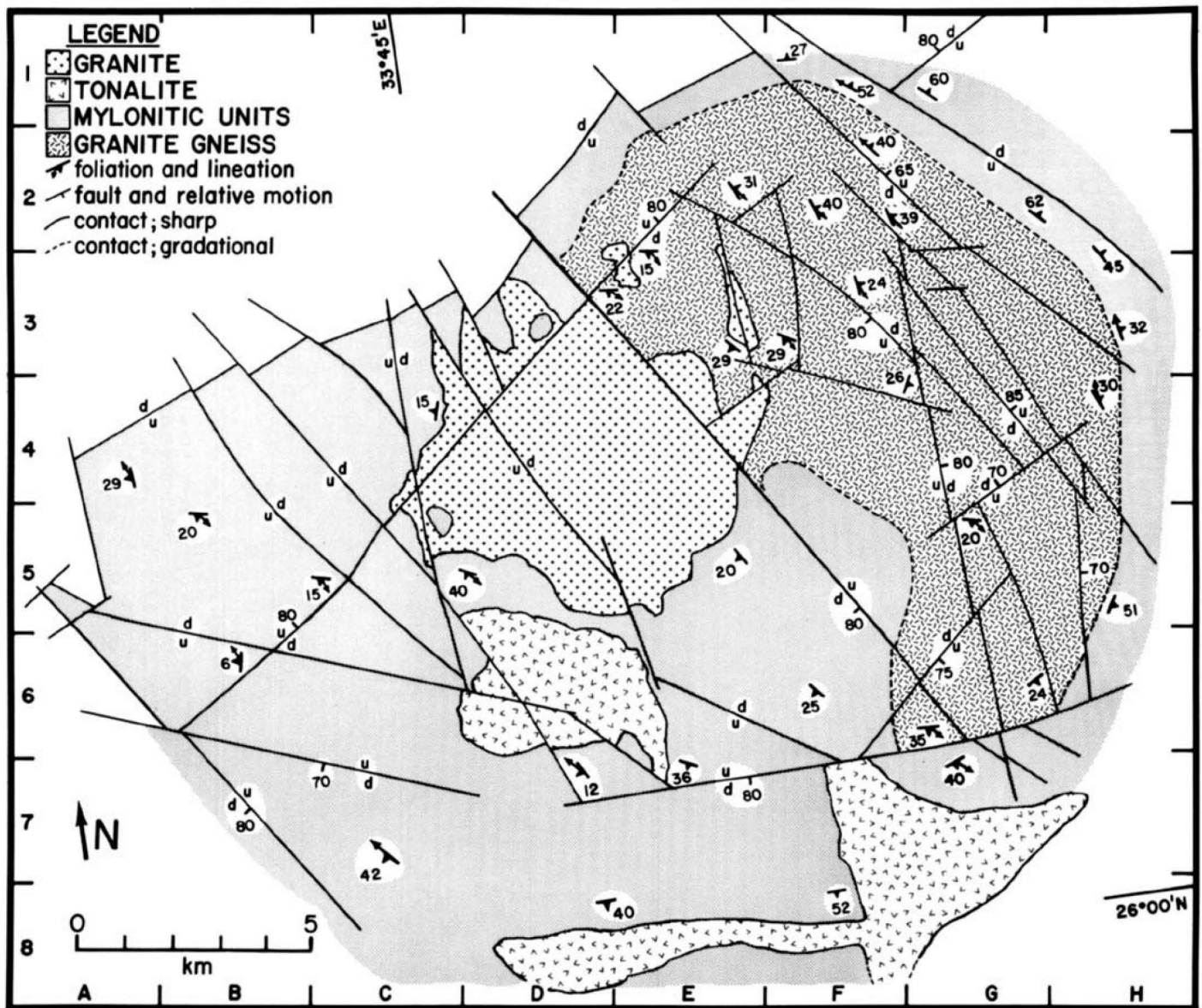


Figure 2. Geological map of Meatiq area adapted from Sturchio and others (1983), compiled on the basis of field observations, aerial photographs, and Landsat multispectral scanner data. Tick marks are added for reference.

mylonite; (3) quartz phyllonite; and (4) a mixture of biotite schist, mafic mylonite, massive to gneissic amphibolite, and serpentinite (Fig. 3) (Sturchio and others, 1983). The thickness of the sequence is estimated to be 2–3 km; approximately two-thirds of the thickness consists of granite gneiss. Syntectonic diorite-tonalite-granodiorite bodies intrude the units, mainly above the granite gneiss, and post-tectonic coarse- and fine-grained granitic rocks crosscut all of the units in the dome (Sturchio and others, 1984; Sturchio and Muehlenbachs, 1985; Sultan and others, 1986c). A detailed discussion of the geologic history of the area is not essential to the scope of this paper and is addressed in the above references. Although only four major units are shown in Figure 2, the major lithologic units described above have been documented from numerous field sampling traverses covering ~300 km. In addition, some 200 samples have been collected and examined petrographically and geochemically. As is shown below, these observations play crucial roles in development of procedures for processing and presenting TM data and in determining the capabilities and limitations associated with lithologic mapping from the processed TM data.

PETROGRAPHIC AND SPECTRAL CHARACTERISTICS OF ROCK TYPES EXPOSED IN THE MEATIQ DOME AREA

In this section, bi-directional reflectances (the fraction of incident light reflected from a surface in the direction of a detector) for powders of fresh samples of Meatiq rocks are interpreted in terms of their respective mineralogies. For reference, modal analyses for the ten major rock units found in the Meatiq dome are given in Table 1, and petrographic descriptions for these rock types are given in Sturchio (1983) and Sultan (1984). Most rock units are quartzofeldspathic in composition, with the exception of the mafic units (mafic mylonite, massive amphibolite) and the ultramafic unit (serpentinite). Chemical analyses for most of these rock types are given by Sturchio and others (1984), Sturchio and Muehlenbachs (1985), and Sultan and others (1986c).

Figure 4 shows bi-directional reflectance data for the powders, acquired using the RELAB spectrophotometer at Brown University (refer to

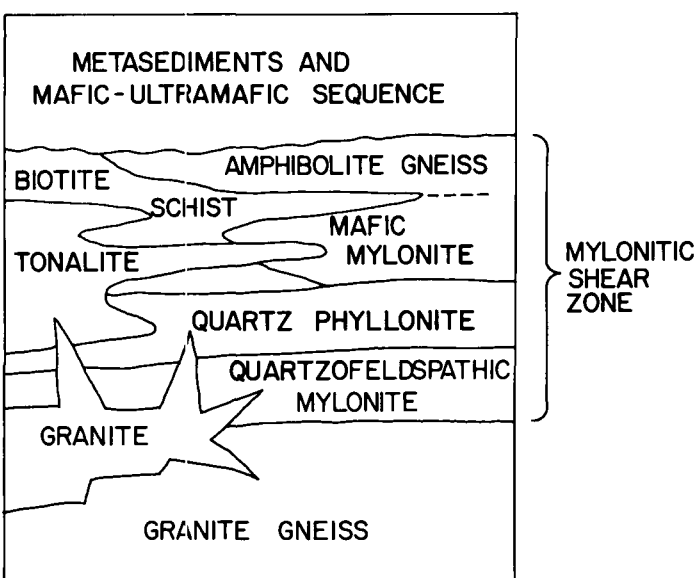


Figure 3. Schematic structural column adapted from Sturchio and Muehlenbachs (1985).

Pieters, 1983, for discussion of the RELAB system). The data were acquired using lighting and viewing geometry specific to the TM data for the Meatiq region (see captions of Figs. 1 and 4). Powders are useful for identifying relations between spectral reflectance and mineralogy. Fine-grained powders have higher reflectances, record relatively deep light penetration into grains, and are generally more homogeneous than natural rock surfaces or sawed slabs on the scale of the incident light beam width (maximum beam width used was ~8 mm). Differences in packing density and other parameters between powders and the rock surfaces that dominate in the Meatiq area render quantitative correlations between laboratory-obtained spectra for powders and TM-based spectra for rock surfaces difficult. In addition, powder reflectances are not modulated by coatings as in the case of natural rock surfaces. Thus, no attempt will be made to quantitatively correlate powder and actual TM data. Rather, the intent is to develop an internally consistent model for relationships between mineralogy and powder spectral reflectance values, concentrating on unique information contained in those wavelengths covered by the TM instrument. In a later section, TM-derived reflectances over homogeneous outcrops of given rock types will be discussed, and evidence will be presented that the same mineralogical controls seen in powder spectra can also be seen in the TM data, although necessarily with different absolute values as compared to the powder data.

Opaque minerals such as magnetite and ilmenite have low, flat reflectance spectra due to iron- and titanium-related overlapping electronic transition and crystal field absorptions (Hunt and others, 1971). Singer (1981) found that addition of only about 5 wt% fine-grained magnetite to rock powders reduces the over-all spectral reflectance and spectral contrast (that is, intensity of absorption features) by approximately a factor of two. Minerals that have low, flat spectral reflectances are defined as "opaque phases" by Hunt and others (1971), and this terminology will be used in the same sense throughout this paper. The importance of opaque phase content as a rock type discrimination tool was shown by Hunt and others (1974). They found that mafic rocks generally have lower spectral reflectances than acidic, intermediate, and ultramafic rocks, due to the relatively high abundance of opaque phases.

Because of the potential importance of opaque-phase content as a rock type discriminator for the Meatiq area, oxide phases in the samples from each of the ten rock types were identified using reflected light microscopy, and scanning electron microscopy/energy dispersive X-ray spectrometry. Predominant oxide phases are (1) titanomagnetite in quartzofeldspathic mylonite, granite gneiss, mafic mylonite, and massive amphibolite; (2) ilmenite in tonalite, coarse-grained granite and fine-grained granite; (3) magnetite in serpentinite; and (4) titanhematite in biotite schist and quartz phyllonite. Microprobe analyses indicate that titanhematite in biotite schist is relatively rich in titanium (~10 wt% TiO₂). Titanium-free hematite has a relatively high reflectance in the near-infrared and is not considered to be an opaque phase (Hunt and others, 1971). Hematite rich in titanium, however, is predicted to be opaque in the near-infrared wavelength region because, as noted by Hunt and others (1971), (1) broad hydrated titanium ion absorptions extend from 0.5 μm into the infrared, with a minimum at 2.0 μm; and (2) Ti substitution in Fe₂O₃ reduces some ferric ions to ferrous ions that in turn produce broad features centered near the 1.5 and 1.8-μm wavelength region. The titanhematite in biotite schist is thus treated as an opaque phase in this work. Based on reflectance data presented in Hunt and others (1971), all other identified oxide phases fall into the opaque category.

Serpentinite contains the highest proportion of opaque phases (~10 vol% magnetite) in the Meatiq dome rocks and shows the lowest over-all reflectance, with minimal spectral contrast (Fig. 4). Granitic rocks (coarse- and fine-grained granites, and granite gneiss), with reduced abundances of

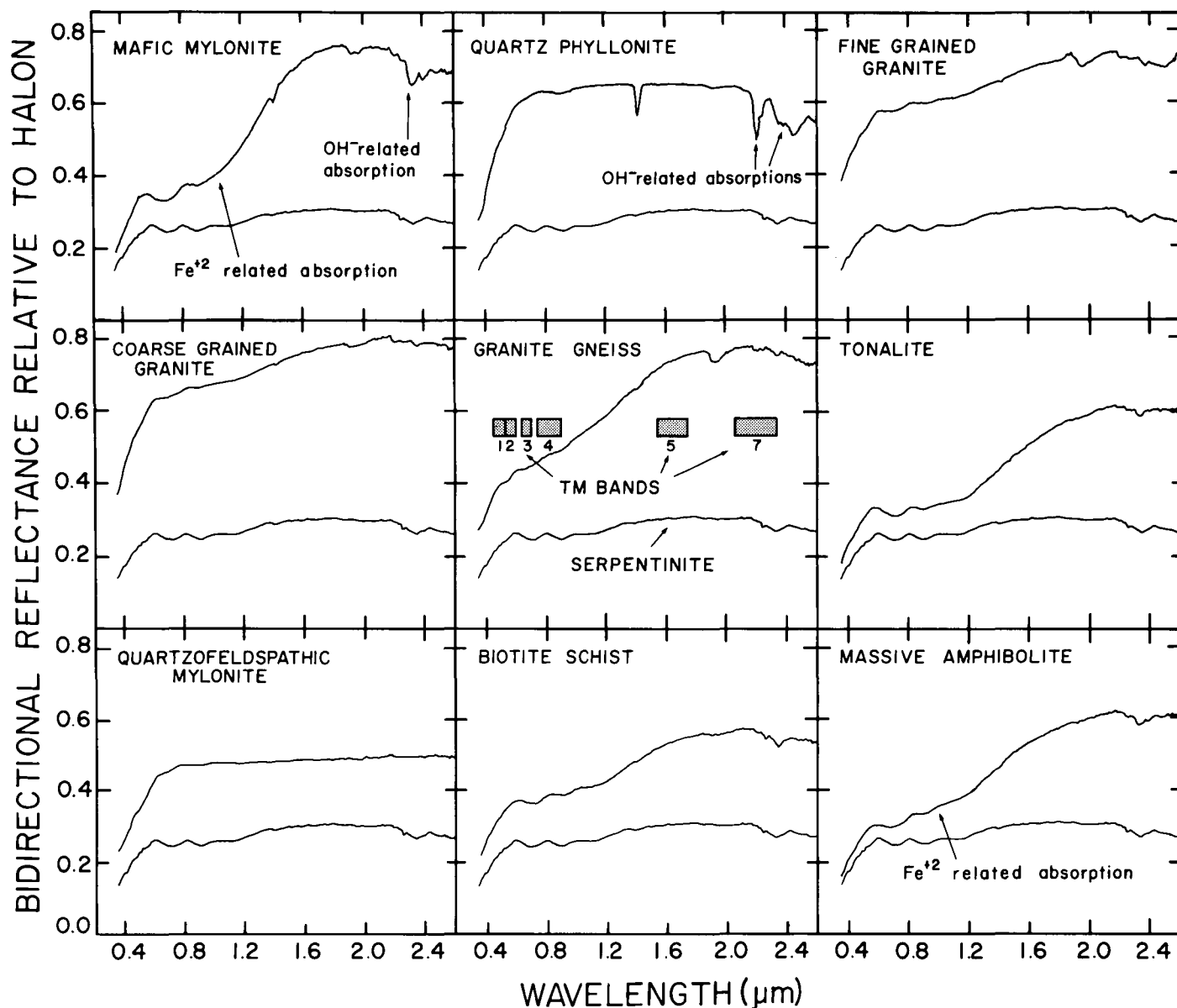


Figure 4. Bi-directional spectral reflectance curves for rock powders. Granite gneiss from sample; massive amphibolite; quartzofeldspathic mylonite; mafic mylonite; biotite schist; coarse-grained granite; fine-grained granite; tonalite; serpentinite. Serpentinite data are shown for reference on all plots. The positions of TM bands are given. Spectral variations induced by grain size variations were minimized by pulverizing representative samples of all rock types to similar grain sizes (range and mean value of grain sizes for each powder is 75–150 μm and 100 μm , respectively). The RELAB system was utilized to acquire the data. The RELAB was run with a spectral sampling interval of 10 nm, a spectral resolution varying from 2 to 14 nm, and a precision of plus and minus 0.25% reflectance. Incidence angle is 30°; 0° emission angle. The data are shown normalized to halon, a gray material that reflects energy equally in all directions.

opaque phases (<1 vol% ilmenite and titanomagnetite), have the highest over-all spectral reflectance values and highest spectral contrast. The effect of opaque phases on reflectance values of powders is also exemplified in the case of mineralogically and chemically similar rock types that differ only with regard to opaque phase content. The quartzofeldspathic mylonite is compositionally and mineralogically similar to the granite gneiss (Table 1), except the mylonite contains more magnetite (~1.5 vol% titanomagnetite) than the gneiss (>0.5 vol% titanomagnetite). The quartzofeldspathic mylonite reflectance curve is also lower in over-all value and

spectral contrast than the curve for the granite gneiss, consistent with the predicted effects associated with opaque phases. Similarly, massive amphibolite contains a higher abundance of opaque phases (~3 vol% titanomagnetite) than do the compositionally and mineralogically similar mafic mylonite (<0.1 vol% titanomagnetite). Again, the massive amphibolite has a lower over-all reflectance as compared to the mafic mylonite.

The vibrational absorptions in the 2.2- to 2.4- μm wavelength region related to combination bands involving the hydroxyl ion fundamental stretching mode has been well documented in the literature (Hunt, 1977;

Hunt and Salisbury, 1970; Hunt and others, 1973a). As seen in Figure 4, rocks rich in hydroxyl-bearing phases and poor in opaque phases (quartz phyllonite with ~30 vol% muscovite, mafic mylonite with ~60 vol% hornblende) strongly absorb in the 2.2- to 2.4- μm wavelength region. Rocks rich in both hydroxyl-bearing phases and opaque phases (serpentinite with ~90 vol% serpentine, talc, and chlorite, and ~10 vol% magnetite; massive amphibolite with ~60 vol% hornblende and ~3.0 vol% titanomagnetite; biotite schist with ~20 vol% biotite and ~2.5 vol% titanhematite) show weaker absorptions in the 2.2- to 2.4- μm wavelength region. This observation is consistent with the role of opaque phases in reducing the intensity of absorption features. On the other hand, rocks poor in hydroxyl-bearing phases (coarse- and fine-grained granites, tonalite, granite gneiss, and quartzofeldspathic mylonite) do not show pronounced absorptions in the 2.2- to 2.4- μm wavelength region, even though they are deficient in opaque phases.

Ferrous-ion crystal field absorptions in Fe-bearing aluminosilicates such as hornblende and biotite produce broad absorption features centered near 1 μm (Hunt and others, 1974; Blom and others, 1980). These absorptions have been consistently reported for mafic and ultramafic rock powders (Hunt and others, 1974; Adams and Filice, 1967; Gradie and others, 1980) and for mafic and ultramafic rock surfaces (Blom and others, 1980). Near-infrared spectra determined for many prominent plutonic-rock constituents such as feldspar, quartz, forsterite, fayalite, and opaque phases confirm that only Fe-bearing aluminosilicates display the prominent 1- μm absorption feature (Blom and others, 1980). The recognition of this feature is important for mapping mafic and ultramafic rocks, because it is the only spectral feature common to these two major rock types but absent or subdued in felsic and most intermediate rocks (Hunt and others, 1973b, 1973c, 1974).

Figure 4 and Table 1 show that rocks with high contents of Fe-bearing aluminosilicates (mafic mylonite, massive amphibolite, each with about 60 vol% hornblende) have broad, deep absorptions near 1 μm . Felsic rocks, with a low abundance of Fe-bearing aluminosilicates (coarse- and fine-grained granite, granite gneiss, quartzofeldspathic mylonite, and quartz phyllonite, each with less than 10 vol%), lack significant absorptions in the 1 μm region. Biotite schist and tonalite, with moderate amounts of biotite and hornblende (10 to 20 vol% combined for each) show evidence

for weak broad absorption in the 1 μm region. Finally, serpentinites, with only minor amounts of Fe-bearing aluminosilicates, show no significant absorptions in this wavelength interval.

PETROGRAPHIC, GEOCHEMICAL, AND SPECTRAL CHARACTERISTICS OF DESERT VARNISH COVERING OUTCROPS

Rock coatings known as desert varnish cover most outcrops in the Meatiq area. Detailed studies of desert varnish from many arid and semi-arid regions (Engel and Sharp, 1958; Adams and others, 1982) indicate that the coatings are characterized by a high concentration of iron, manganese, and magnesium relative to the host rock (Allen, 1978). Clay minerals with strong hydroxyl-related absorptions are major phases in many desert varnish coatings (Potter and Rossman, 1977). As mentioned above, strong absorption features are related to iron-bearing phases and hydroxyl-bearing phases. Therefore, a clear understanding of varnish distribution and mineralogy in relation to the underlying rocks in the Meatiq area is necessary to evaluate its contribution to the data acquired by the TM instrument.

In the Meatiq area, outcrops of coated felsic rocks are brighter than those of mafic and ultramafic rocks. Rarely is the surface coating thick enough to mask the underlying host rock, as coatings are generally thin and discontinuous, allowing visual identification of the respective rock mineral constituents. In addition, there is no apparent systematic variation in coating thickness among rock types or with location, based on visual examination of many outcrops and thin sections.

Thin sections of coatings from each of the ten major rock types listed in Table 1 were examined using transmitted light microscopy and back-scattered electron images (Fig. 5). The following textural observations were made: (1) rock coatings are generally very thin (0–5 μm), although they may be thicker (up to 50 μm) in local rock surface depressions; (2) a sharp contact always separates the coatings from the host rocks; (3) coatings are either amorphous or very fine-grained (<1 μm); and (4) larger grains (1 to 10 μm) are irregularly distributed in the coatings. Some of these larger grains may have originated from the host rock, whereas some have an external provenance as in the case of quartz grains found in a coating on a massive amphibolite devoid of quartz.

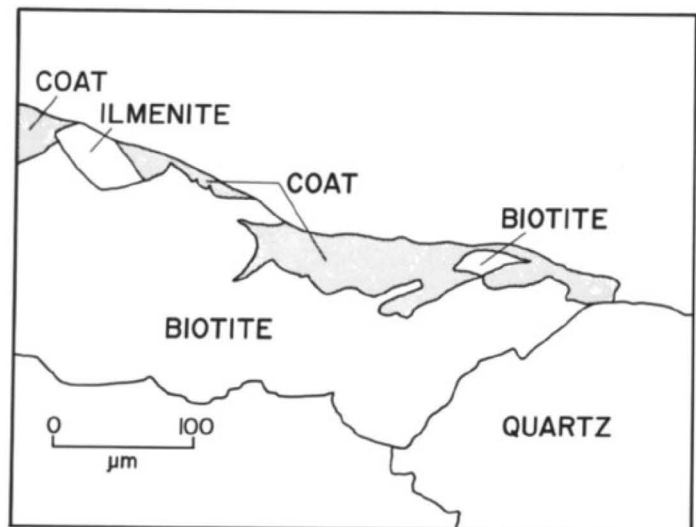
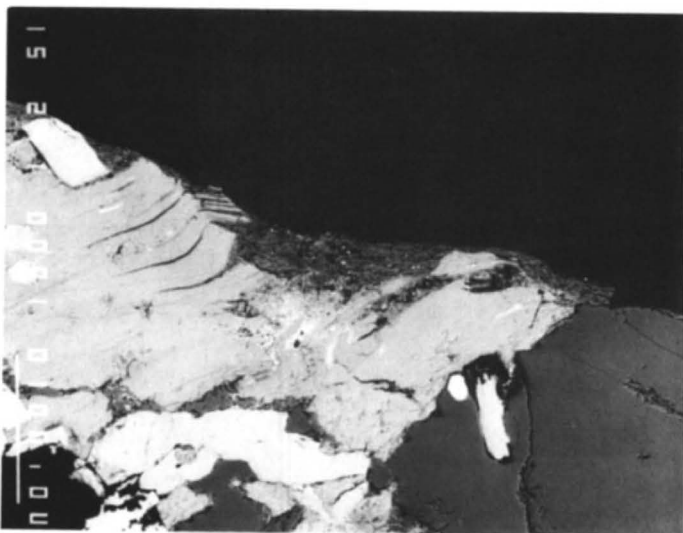


Figure 5. Left: compositional microprobe image for coating from a coarse-grained granite. Right: interpretation sketch for the compositional image.

TABLE 1. AVERAGE MODAL ANALYSES OF 2 TO 5 REPRESENTATIVE SAMPLES FROM EACH ROCK TYPE

Rock type	Qz	Pl	Kf	Mu	Bi	Ch	Gt	Am	Mt	Hm	Il	Sp	Ep	Cc	Se	T
Granite gneiss	34	32	26	..	3	tr	..	5	tr	..	tr	tr	tr
Quartzofeldspathic mylonite	38	30	28	tr	2	tr	tr	..	2	..	tr	tr	tr
Quartz phyllonite	61	..	8	29	2	..	tr	tr	..	tr	tr
Biotite schist	42	27	..	4	18	4	1	4	tr
Mafic mylonite	tr	34	64	tr	2
Massive amphibolite	2	25	5	tr	..	65	3	tr	tr
Coarse-grained granite	35	32	30	..	3	tr
Fine-grained granite	35	34	29	..	2	tr
Tonalite	14	72	tr	..	11	tr	1	1	1	tr
Serpentine	3	10	2	80	5

Abbreviations: Qz = quartz; Pl = plagioclase; Kf = K-feldspar; Mu = muscovite; Bi = biotite; Ch = chlorite; Gt = garnet; Am = amphibole; Mt = magnetite or titanomagnetite; Hm = titanhematite; Il = ilmenite; Sp = sphene; Ep = epidote; Cc = calcite or magnesite; Se = serpentine; T = talc; tr = <1%; .. = not observed;
 Note: accessory phases not included.
 Data from point counts of thin sections, Sturchio (1983), and Sultan (1984). Amphibolite gneiss and massive amphibolite were grouped in a single unit referred to as massive amphibolite throughout the text, as these rocks are compositionally and spectrally similar and are in proximity in the field. Serpentine-magnetite-talc-chlorite-carbonate rocks are referred to as serpentinites throughout the text.

The composition of coatings overlying a coarse-grained granite, a tonalite, and a massive amphibolite was determined using energy-dispersive microprobe analysis. The analyses of the coatings along with whole-rock analyses for underlying rocks are presented in Table 2. Analyses were performed using a 5- μ m beam width for areas that have the thickest coats (at least 10 μ m). For each coating, the range of major-element abundances taken along traverses running parallel to the rock

surface and ~200 μ m in length, are reported. Results demonstrate that the individual coatings are compositionally heterogeneous. These heterogeneities may reflect the irregular distribution of incorporated grains seen in thin sections and in backscatter compositional images. In addition, the composition of the coatings does not seem to vary systematically with the composition of the host rocks. This conclusion is supported by the overlap in the ranges of variations for most of the analyzed major-element abundances (Table 2).

TABLE 2. CHEMICAL ANALYSES OF DESERT VARNISH AND UNDERLYING ROCKS FOR SEVERAL SAMPLES

	Coarse-grained granite			Tonalite			Massive amphibolite		
	R	Min	Max	R	Min	Max	R	Min	Max
SiO ₂	74.0	34.5	38.9	64.7	35.8	40.5	48.2	38.0	42.6
Al ₂ O ₃	13.3	19.9	22.0	16.2	18.9	19.3	15.2	18.2	20.6
FeO*	1.22	7.5	10.8	3.9	6.7	7.9	10.3	7.9	9.4
TiO ₂	0.16	1.2	1.6	0.69	0.7	1.0	1.05	0.9	5.6
MnO	0.01	2.0	3.1	0.08	4.4	8.5	0.2	1.4	2.6
MgO	0.33	6.2	13.5	1.94	5.2	6.6	6.95	3.4	4.4
CaO	1.0	0.7	2.5	3.19	0.7	1.0	12.1	1.3	2.4
Na ₂ O	3.57	0.2	0.3	4.49	0.0	0.3	2.08	0.0	0.8
K ₂ O	4.73	0.9	1.2	2.82	1.3	1.6	0.52	1.1	1.2
LOI	1.1	n.d.	n.d.	1.3	n.d.	n.d.	2.6	n.d.	n.d.

Analysis R is for underlying rock determined by X-ray fluorescence, using an automated Siemens SRS-2000 X-ray spectrometer, following the technique outlined by Norrish and Hutton (1969). Range (min-max of three analyses) of major-element abundances in the overlying coat was obtained using a fully automated JEOL 733 Superprobe, an accelerating voltage of 15 Kv, a current of 20 nanoamps, and a beam diameter 5 μ m.

*Total Fe as FeO. n.d. not determined.
 XRD patterns were obtained for coatings separated from coarse-grained granite and massive amphibolite thin sections. Thin (0.4 mm in thickness) saw blades were used in preparation of thin sections to preserve coats. Fifty μ m-thick coatings were attached to a glass fiber, and an XRD pattern was obtained using a Debye-Scherrer camera.

The mineralogy of the coatings was examined using X-ray diffraction (XRD) patterns for thick coatings (50 μ m) separated from massive amphibolite and coarse-grained granite thin sections (refer to caption of Table 2 for applied procedures). XRD patterns for the massive amphibolite coating confirmed the presence of a poorly crystalline dioctahedral smectite phase. An XRD analysis of a coating from the granite sample showed only an amorphous halo. Fe and Fe-Ti oxides and/or oxyhydroxides, but not Mn oxides, are present in coatings on massive amphibolite, tonalite, and coarse-grained granite, on the basis of energy-dispersive microprobe analyses. Average modal abundances (<3 vol%) of Fe and Fe-Ti oxides and/or oxyhydroxides in coatings of these three rock types were obtained by counting the bright spots on compositional images, using the reasonable assumption that all bright spots are formed of these oxides and/or oxyhydroxides. The brightest areas on compositional images should correspond to minerals with the highest atomic numbers. The low abundance of Fe and Fe-Ti oxides and/or oxyhydroxides, coupled with the consistent clay-like elemental abundances for most of the analyzed spots, indicates that amorphous to poorly crystalline clay-like material is probably the main constituent of the examined coatings. Similar textural and compositional

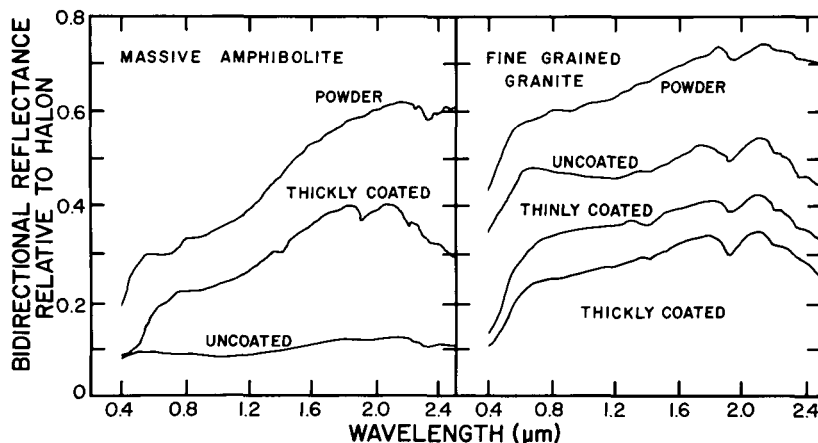


Figure 6. Bi-directional spectral reflectance data relative to halon for powder, and for thickly coated, thinly coated, and uncoated surfaces from massive amphibolite and fine-grained granite acquired using RELAB. Incidence angle is 30°; 0° emission angle.

observations led workers to suggest that desert varnish elsewhere is composed largely of wind-blown products (Potter and Rossman, 1977, 1979; Allen, 1978; Adaras and others, 1982).

The extent to which the rock coatings modify the spectral reflectances of fresh Meatiq rocks was addressed by examining bi-directional reflectances measured for powders, and for thickly coated, thinly coated, and uncoated surfaces of massive amphibolite and fine-grained granite samples (Fig. 6). The spectral data for massive amphibolite show the following. (1) Two water-related absorption features centered near 1.4 and 1.9 μm in the coated slab, consistent with the presence of a smectite phase in the coating and its absence in the underlying rock; (2) hydroxyl-related absorptions centered at 2.35 μm in data for all massive amphibolite spectra, consistent with the abundance of amphiboles; (3) combined strong hydroxyl-related absorptions centered at 2.2 and 2.35 μm , observed only in the spectra for the coated surface and thus probably due to presence of smectite; (4) broad ferrous-related absorption near the 1- μm area in all of the massive amphibolite spectra; and (5) increase in over-all spectral reflectance values and spectral contrast from uncoated to the coated surfaces. The fine-grained granite spectra (Fig. 6) show the following features. (1) Narrow absorptions centered at 1.4 and 1.9 μm , possibly resulting from one or more of the following: fluid inclusions common in granitic magmas, adsorbed water, or bound water in the smectites of the coated surface; (2) hydroxyl-related absorptions related to the sericitization of feldspar, or to the presence of clay minerals in the coating; (3) absence of the ferrous-related absorption observed in the massive amphibolite data; and

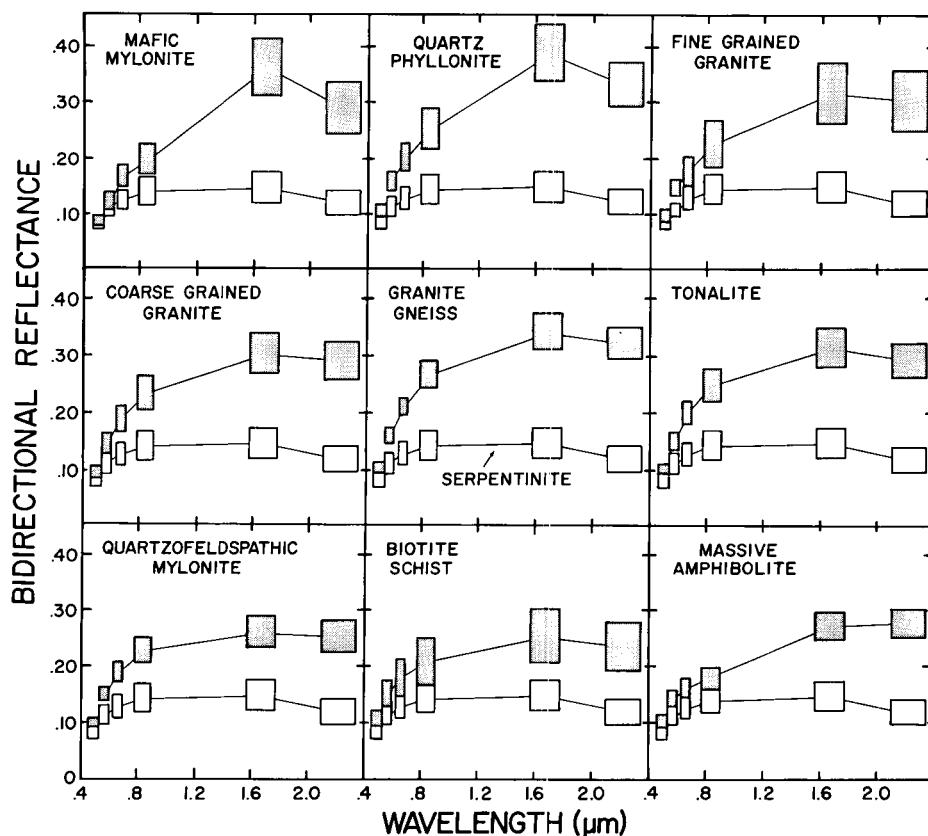
(4) decrease in over-all spectral reflectance and contrast from uncoated to coated surfaces.

Examination of Figure 6 indicates the following. (1) The broad ferrous-related absorption is not obscured, even for the thickest coatings. (2) Coated mafic rocks are brighter and have higher spectral contrast as compared to natural uncoated surfaces, whereas coated felsic rocks are generally darker and show lower over-all contrast than uncoated surfaces. Thus, thick coatings can obscure differences in over-all spectral reflectance and contrast between some uncoated mafic and felsic surfaces by increasing the contrast for mafic rocks, but decreasing that of felsic units. (3) Clay minerals in the coatings strongly absorb in the 2.2- 2.35- μm wavelength region and contribute to the hydroxyl-related absorption feature. We cannot evaluate by only examining the laboratory-obtained spectra addressed above whether the coatings in the Meatiq dome area are volumetrically important to obscure the hydroxyl-related and opaque phase-related absorptions. Rather, TM data over well-known outcrops with varying hydroxyl ion and opaque phase contents need to be examined.

TM REFLECTANCE VALUES AND PROCESSING PROCEDURES

TM-derived bi-directional reflectance data for outcrops for each of the ten major rock types are shown in Figure 7. The data plotted in Figure 7 were derived from homogeneous outcrops (test sites) for each rock type, areas where detailed field observations ensure no mixing of

Figure 7. Representative TM spectral reflectance data for the major rock units acquired over the test-site outcrops discussed in the text. Sample sites cover 0.2 km² on the average. Approximate locations of the test-site outcrops in Figure 8 are as follows: granite gneiss, F2; quartzofeldspathic mylonite, F5; quartz phyllonite, B5; mafic mylonite, H3; massive amphibolite, H1; biotite schist, E7; coarse-grained granite, E4; fine-grained granite, D4; tonalite, D6; serpentinite upper left of A1 (not shown). The serpentinite data are plotted with each of the other data sets for reference. The width of the TM boxes is equivalent to the band width, and the height is plus/minus one standard deviation about the mean value for the test-site outcrops. Reflectance values were computed using the following procedure: (1) gain and offset parameters (Barker and others, 1985) were applied in each band; (2) values over a homogeneous portion of the Red Sea were used to estimate the additive atmospheric radiance term for the over-all scene, assuming that the Red Sea reflectance was typical for clear (non-turbid), deep water; (3) the additive term was removed from each picture element for each band; and (4) the corrected radiance values were normalized by the solar irradiance term, integrated over the appropriate band passes. The resultant data are proportional to surface bi-directional reflectance multiplied by an attenuation factor due to extinction of light by atmospheric absorption and scattering. No further corrections were made because the relative variations of interest should be largely independent of any broadly wavelength-dependent factors associated with atmospheric extinction.



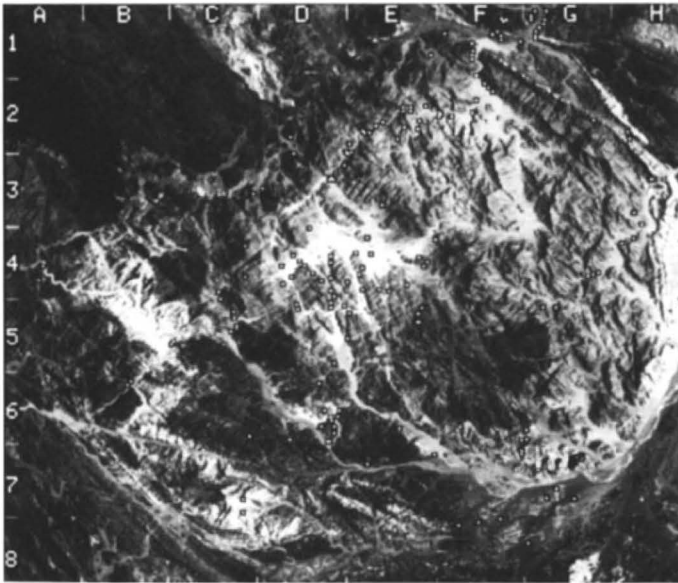


Figure 8. TM band-5 image for same region covered by Figure 2. Tick marks and sample locations (boxes) are added for reference.

units. The reflectance data were generated by converting the brightness value in each image to reflectance values using procedures described in the caption of Figure 7.

The Meatiq test area exhibits considerable topographic relief (the range in elevations is ~1,000 m), demanding a TM-data processing procedure that suppresses variations in reflectance due to variations in slope angles and azimuths. The rugged nature of the terrane is clearly shown in the raw TM band-5 image shown in Figure 8. Reflectance ratios have been found to suppress variations due to topography and to variations in overall reflectance, while emphasizing differences in shapes of spectral reflectance curves (Rowan and others, 1975; Abrams and others, 1977). As differences in grain size are thought to primarily produce shifts in overall reflectance (Adams and Filice, 1967), ratioing should also suppress brightness differences related to grain size variations. Ratioing of TM bands was therefore chosen as an integral part of the processing procedures. In the next three sections, ratios are described that emphasize variations related to the three dominant mineralogical controls that are apparent in the powder reflectance data and that should be apparent in the TM-derived reflectance data if coatings and weathering products do not obscure the reflectance of the underlying rock.

TM BAND-5/1 RATIO AND OPAQUE PHASES

TM band 5 (1.55–1.75 μm) lies between major vibrational absorptions at longer wavelengths (1.9, 2.2–2.4 μm) and major charge transfer and conduction bands due to Fe-bearing aluminosilicates at shorter wavelengths ($\leq 1.0 \mu\text{m}$). Generally, reflectance values should be high for the band-5 region, except for rocks with high contents of opaque phases (for example, serpentinites) (Fig. 7). A ratio of band 5 to 1 should portray the broad over-all reflectance value, because band 1 (0.42 to 0.55 μm) is located in the wavelength region where reflectances are ubiquitously very low because of intense charge transfer and conduction band absorptions in materials with even trace amounts of iron (Hunt, 1977). Rocks rich in opaque phases should therefore have low band-5 and band-1 values, whereas other rocks should have high band-5 and low band-1 values.

The abundance of Fe-bearing aluminosilicates might produce a similar, yet smaller effect in reducing the over-all spectral reflectance and contrast, if the Fe-related absorptions were strong enough to extend in the band-5 wavelength region (Hunt and others, 1973a; Adams, 1975). Examination of powder reflectance spectra of mafic mylonite (Fig. 7), the rock type with the highest amount of Fe-bearing aluminosilicates (~60 vol% hornblende) and the lowest amount of opaque phases (<0.1 vol% titanomagnetite), indicates that the broad ferrous-related absorption centered near 1 μm does not significantly reduce the spectral contrast and band-5 reflectance values. In fact, it will be shown that mafic mylonites have the highest TM band-5/1 values. Ti-free hematite, goethite, and other transopaque phases that strongly absorb in the band-1 wavelength region but not in the band-5 wavelength region can increase the value of TM band-5/1 ratios (Abrams and others, 1977). Inspection of Table 1 shows that these transopaque phases are not major phases in any of the Meatiq rock types. Highly weathered surfaces rich in transopaque phases are rare, according to field observations.

Figure 9A shows TM band-5/1 reflectance ratios extracted from the test sites plotted against modal opaque phase content for representative samples. Figure 10A is a band-5/1 image for the Meatiq test area. Comparison of Figures 8 and 10A clearly shows the value of band ratioing for suppressing spectral variations related to topography and to grain sizes. Inspection of Figure 9A indicates a general trend of increasing TM band-5/1 value with decreasing opaque phase content. The trend demonstrates that varnish and weathering products do not obscure the opaque phase control on bi-directional reflectance values derived from TM data.

Major rock types have been documented along numerous field traverses covering ~300 km within the dome area. These traverses were drawn on 1:10,000 aerial photographs during the course of field work. Traverses are shown in Figure 10D at the same scale as the band-5/1 image, with an accuracy in location of ~100 m. The identification of rock types along the traverses was based on petrographic examination of all collected samples (200 samples) and whole-rock major-element analyses acquired for 30% of the collected samples. Examination of traverse and sample data and TM band-5/1 image indicates that the Meatiq rocks can be visually divided into three groups on the basis of their opaque phase content and their corresponding brightness in TM band-5/1 image. These broad divisions and similar ones applied to the two other ratio images are done mainly for the convenience of the reader. (1) Rocks with a low abundance of opaque phases (<1.0 vol%) and high 5/1 values (mafic mylonite, quartz phyllonite, coarse- and fine-grained granites, granite gneiss, and tonalite). (2) Rocks with moderate contents of opaque phases (between 1.0 and 3.5 vol%) and moderate 5/1 values (quartzofeldspathic mylonite, massive amphibolite, and biotite schist). (3) Rocks with high abundance of opaque phases (>3.5 vol%) and low 5/1 values (serpentinite). For example, note that massive amphibolite is darker in band-5/1 image along southeast-northwest-trending traverses in sections G1 and G2 (Fig. 10A) compared to fine-grained granite along traverses trending north-south and northwest-southeast in sections D4 and D5. Neither the varnish nor the weathering products seem to strongly influence the band-5/1 reflectance values.

TM BAND-5/7 RATIO AND HYDROXYL-BEARING PHASES

Reflectances in the TM band-7 spectral region (2.08 to 2.35 μm) must be at least partially dependent on the hydroxyl content of the rocks. The ratio of bands 5 to 7 was used as a measure of the intensity of the hydroxyl absorptions in the 2.2–2.4 μm region. This ratio was used because, as noted, band 5 is not within the confines of the Fe-bearing

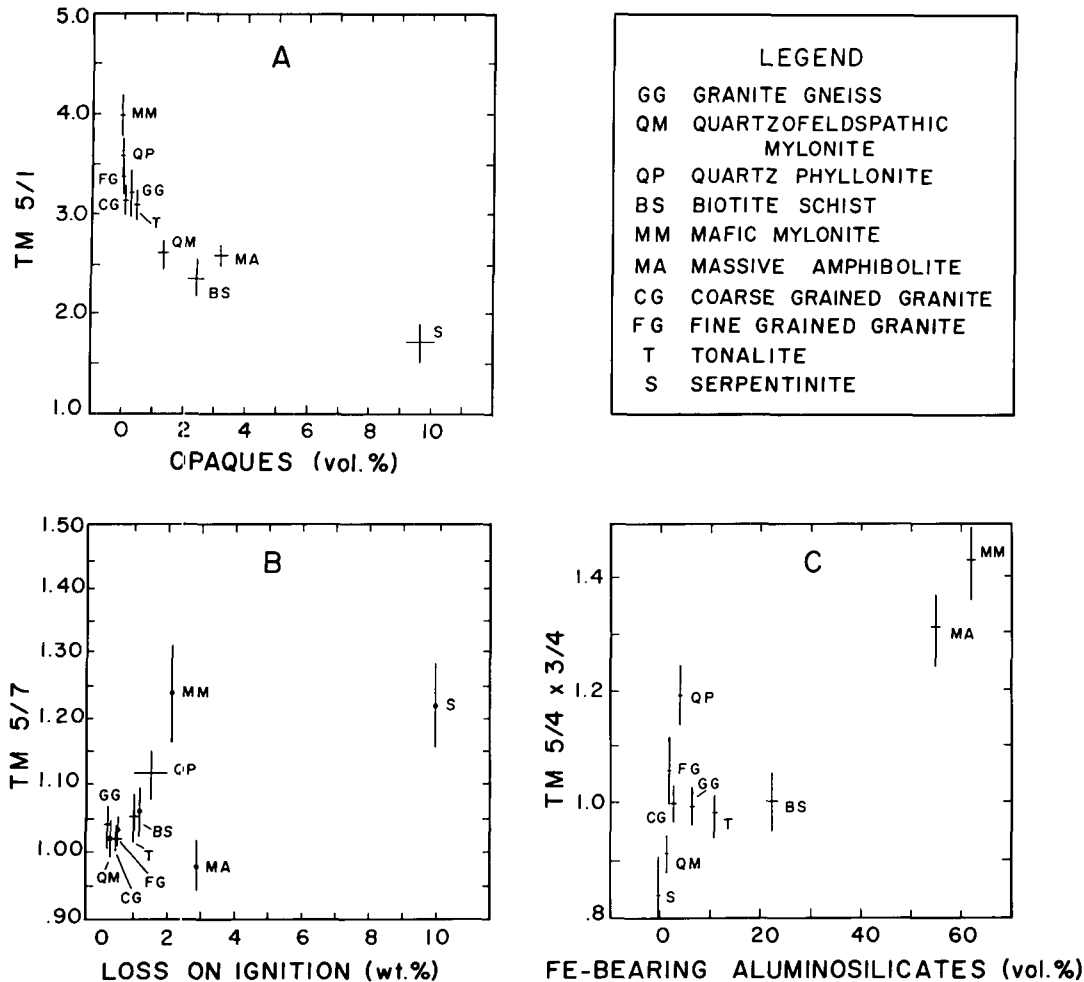


Figure 9. TM band ratios for the test-site outcrops of Figure 7 plotted against vol% opaques (9A), LOI values in wt% (9B), and vol% Fe-bearing aluminosilicates for representative samples (9C). Modal abundances were determined from point counts of 2-5 representative thin sections of each of the major rock types. LOI values were measured for 2 to 11 representative samples for each rock type. Uncertainties in modal abundances represent one standard deviation and are based on counting statistics following procedures described in Van Der Plas and Tobi (1965). Uncertainties are reported only where six or more LOI measurements were made for a single rock type. Uncertainties in TM data represent spread shown in Figure 7. Abbreviations for major rock units are given.

aluminosilicate-related or hydroxyl-related absorption features, whereas band 7 is within the hydroxyl absorption wavelengths. A similar ratio was successfully used to map hydrothermally altered rocks rich in hydroxyl-bearing phases in the southwestern United States (Abrams and others, 1977). Other minerals that also absorb in the band-7 wavelength region, such as pyroxenes and carbonates (Hunt and Salisbury, 1971; Adams, 1975), are not major phases in any of the Meatiq rocks (Table 1). In the Meatiq area, weathering does not seem to significantly modify band-5/7 values. This inference is supported by the paucity of highly weathered surfaces based on field observations and by the absence of strong hydroxyl-related absorptions in TM-data for granites (Fig. 7).

To test the correlation between the hydroxyl content of the Meatiq rocks and the band-5/7 ratio, estimates were determined for the hydroxyl contents of representative fresh samples by measuring the weight loss on ignition (LOI) following procedures described in Jeffery (1975). The apparent decrease in LOI values due to the oxidation of iron (ferrous to ferric) was corrected using whole-rock FeO contents determined with the modified Pratte method described in Maxwell (1968). These LOI corrections were performed only for the mafic mylonite and massive amphibolite, because these are the units containing considerable amounts of iron (~10 wt%).

LOI data show that serpentinite, mafic mylonite, massive amphibolite, biotite schist, and quartz phyllonite are relatively rich in hydroxyl-

bearing minerals, consistent with mineral modes (Table 1). On the other hand, coarse- and fine-grained granite, tonalite, granite gneiss, and quartzofeldspathic mylonite are poor in these phases. These trends are shown in Figure 9B, which is a plot of the band-5/7 ratio for the test site outcrops of Figure 7 versus the LOI values. Meatiq rocks that contain small or moderate amounts of opaque phases (granite gneiss, coarse- and fine-grained granite, tonalite, quartz phyllonite, quartzofeldspathic mylonite, biotite schist, and mafic mylonite) show a generally good correlation between LOI numbers and the band-5/7 ratio values. On the other hand, rocks richest in opaque phases (massive amphibolite and serpentinite) exhibit band-5/7 ratios below the main trend, consistent with the role of opaque phases in reducing spectral contrast. Again, the low band-5/7 values for granites support the assumption that coatings do not obscure the hydroxyl-content information of the rocks.

Figure 10B is a band-5/7 ratio image. Examination of traverse and sample data and the TM band-5/7 image indicates that Meatiq rocks with low to moderate content of opaque phases can be visually divided into three groups on the basis of band-5/7 and corresponding LOI values: (1) rocks with high LOI (>2 wt%) and high band-5/7 values (mafic mylonite); (2) rocks with moderate LOI (1.2-1.6 wt%) and band-5/7 values (quartz phyllonite and biotite schist); and (3) rocks with low LOI (<1 wt%) and band-5/7 values (tonalite, coarse- and fine-grained granite, quartzofeldspathic mylonite, and granite gneiss). Despite the opaque

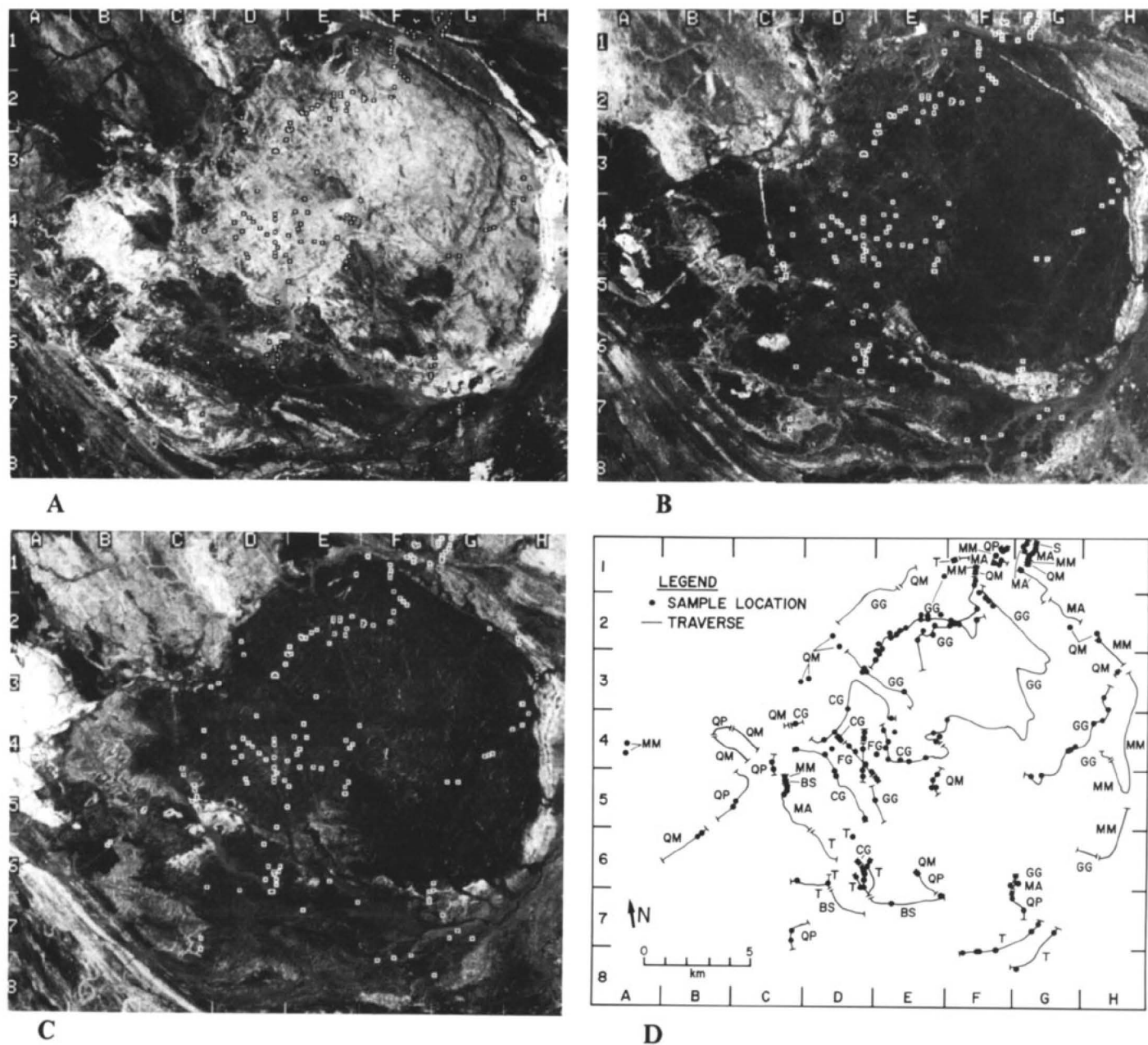


Figure 10. TM band ratio images for the area covered in Figure 2. A. TM band-5/1 image. Bright areas correspond to regions deficient in opaque phases. B. TM band-5/7 image. Bright areas correspond to regions with high hydroxyl contents. C. TM band-5/4 \times 3/4. Bright areas correspond to regions rich in Fe-bearing aluminosilicates. D. Map showing locations traversed by authors during the course of field work and locations (dots) where samples were collected. Sample locations (boxes) and tick marks are added for reference. Sample locations are marked by the center of the dots. Only sample locations that are representative of outcrops covering an area of at least one TM image element (30 m by 30 m) are shown. Specifically, samples from outcrops that are formed of metre-scale intercalations of two or more rock types were excluded, whereas samples that formed approximately 80% or more by area of an outcrop (estimated visually in the field) were included.

phase-induced reduction of the strong hydroxyl-related absorptions in serpentinite, relatively high band-5/7 ratios occur due to the high content of serpentine and other hydroxyl-bearing minerals. Serpentinites in Figure 10B are thus as bright as the rocks in the first group. Massive amphibolite has a considerably lower hydroxyl content as compared to serpentinite and thus shows lower band-5/7 values. They are as dark as rocks in the third group in Figure 10B.

TM BAND-5/4 \times 3/4 RATIO AND IRON-BEARING ALUMINOSILICATES

Examination of TM-derived reflectances for test site outcrops (Fig. 7) shows that only the mafic rocks (massive amphibolite and mafic mylonite) have enough Fe-bearing aluminosilicates to cause a flat or concave-upward spectral reflectance pattern in the band-4 wavelength

region. This pattern must be due, as in the powders, to the broad absorptions associated with ferrous-related absorptions centered near $1 \mu\text{m}$. Baird (1984a, 1984b, 1984c) successfully predicted the iron content of granitic rocks by examining the slopes of the near-infrared spectra between 1 and $2 \mu\text{m}$. These slopes are strongly controlled by ferrous-related absorptions common in Fe-bearing aluminosilicates (Baird, 1984b). A technique similar to one used by Guinness and others (1987) was employed to emphasize the degree of curvature of the reflectance in the band-4 wavelength interval. The product of TM band ratios 5/4 and 3/4 should be high for rocks rich in Fe-bearing aluminosilicates (for example, mafic mylonite and massive amphibolite) as compared to rocks that are relatively deficient in these phases.

Figure 9C is a plot of modal abundance of Fe-bearing aluminosilicates versus band-5/4 \times 3/4 values extracted from the test-site outcrops. A TM band-5/4 \times 3/4 image is shown in Figure 10C. The brightest areas in the image correspond to known outcrops of mafic rocks shown on Figure 10D, whereas the dark areas correspond to the felsic, intermediate, and ultramafic rocks. Inspection of Figures 9C, 10C, and 10D indicates that Meatiq rocks can be visually divided into two groups on the basis of Fe-bearing aluminosilicates and corresponding 5/4 \times 3/4 ratios: (1) mafic rocks; namely, mafic mylonite and massive amphibolite, which have approximately 60 vol% of Fe-bearing aluminosilicate phases; and (2) felsic, intermediate, and ultramafic rocks; namely, coarse- and fine-grained granites, granite gneiss, tonalite, quartzofeldspathic mylonite, quartz phyllonite, serpentinite, and biotite schist, which have less than 25 vol% of Fe-bearing aluminosilicates.

TM BAND RATIO DATA AS A COLOR COMPOSITE

In this section, the lithologic information contained in the three TM band ratio images is integrated into one image product for the purpose of identifying and mapping rock types. Figure 11 shows scatter plots of TM band ratios 5/1, 5/7, and 5/4 \times 3/4 for each of the ten test-site outcrops. Serpentinites are the most readily identified rock type because ratio values for serpentinites are clearly separated from those of all other units. In fact, serpentinites were successfully mapped in more than 60,000 km^2 in the Eastern Desert from two TM scenes by employing simple ratio thresholds (Sultan and others, 1986b). Mafic rocks (massive amphibolites and mafic mylonites) are also separated from the other units, particularly by the band-5/4 \times 3/4 data. Mafic rocks associated with serpentinites forming an extensive ophiolitic mélangé (Shackleton and others, 1980) in the Eastern Desert of Egypt were also mapped on the basis of their brightness in the band-5/4 \times 3/4 image (Sultan and others, 1986a). The above-mentioned rock types thus have unique brightness patterns on the ratio images and should have unique colors on a color composite generated from the three ratio images. Biotite schist, quartzofeldspathic mylonite, and quartz phyllonite show considerable overlap with other units in one or two, but not all the scatter plots, and thus are also readily mapped visually from the color composite. Coarse- and fine-grained granites, tonalite, and granite gneiss cluster tightly around each other in the scatter plots and will have similar brightnesses on the three ratio images and similar colors in the composite. Mapping these rock types as separate units will therefore be difficult, except in locations where detailed field data provide local verification.

A color composite constructed from the three ratio images is shown in Figure 12. The band-5/1 image was assigned the green component; the

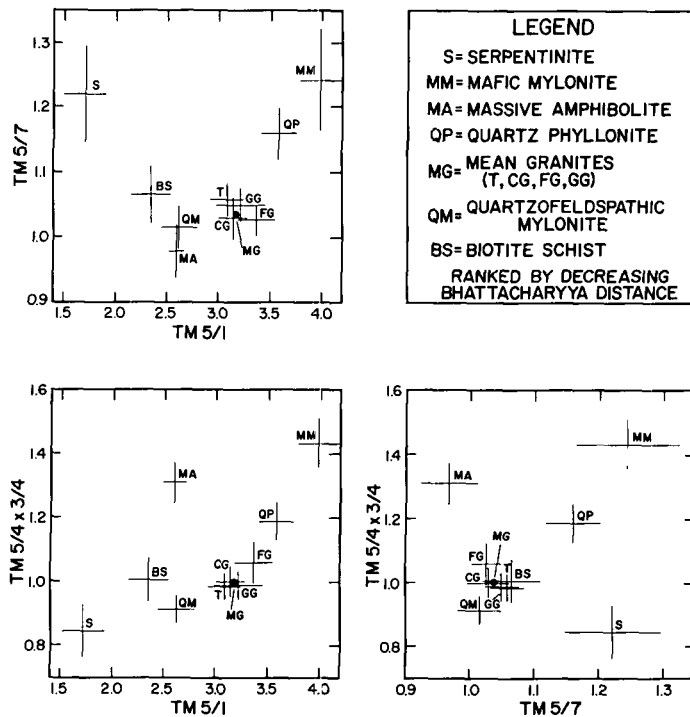


Figure 11. Scatter plots of TM band ratios 5/1, 5/7, and 5/4 \times 3/4 for the test-site outcrops. Uncertainties represent one standard deviation variations in band ratio values over test site outcrops. Rock types are ranked in the legend in decreasing order of statistical separability, using the average of pair-wise Bhattacharyya distances. Bhattacharyya distance measures the statistical separability of two probability density functions (Kailath, 1967). Higher values correspond to greater separability. Rock abbreviations are given in Figure 9.

TABLE 3. EXPLANATION OF RELATIVE COLOR VALUES IN FIGURE 12

Rock type	Band-5/7 image bright = red	Band-5/1 image bright = green	Band-5/4 \times 3/4 image bright = blue	Color in composite image
Granite gneiss	Dark	Bright	Dark	Green
Quartzofeldspathic mylonite	Dark	Moderate	Dark	Dark green
Quartz phyllonite	Moderate	Bright	Dark	Yellow
Mafic mylonite	Bright	Bright	Bright	White
Massive amphibolite	Dark	Moderate	Bright	Blue
Biotite schist	Moderate	Moderate	Dark	Brownish red
Coarse-grained granite	Dark	Bright	Dark	Green
Fine-grained granite	Dark	Bright	Dark	Green
Tonalite	Dark	Bright	Dark	Green
Serpentinite	Bright	Dark	Dark	Red

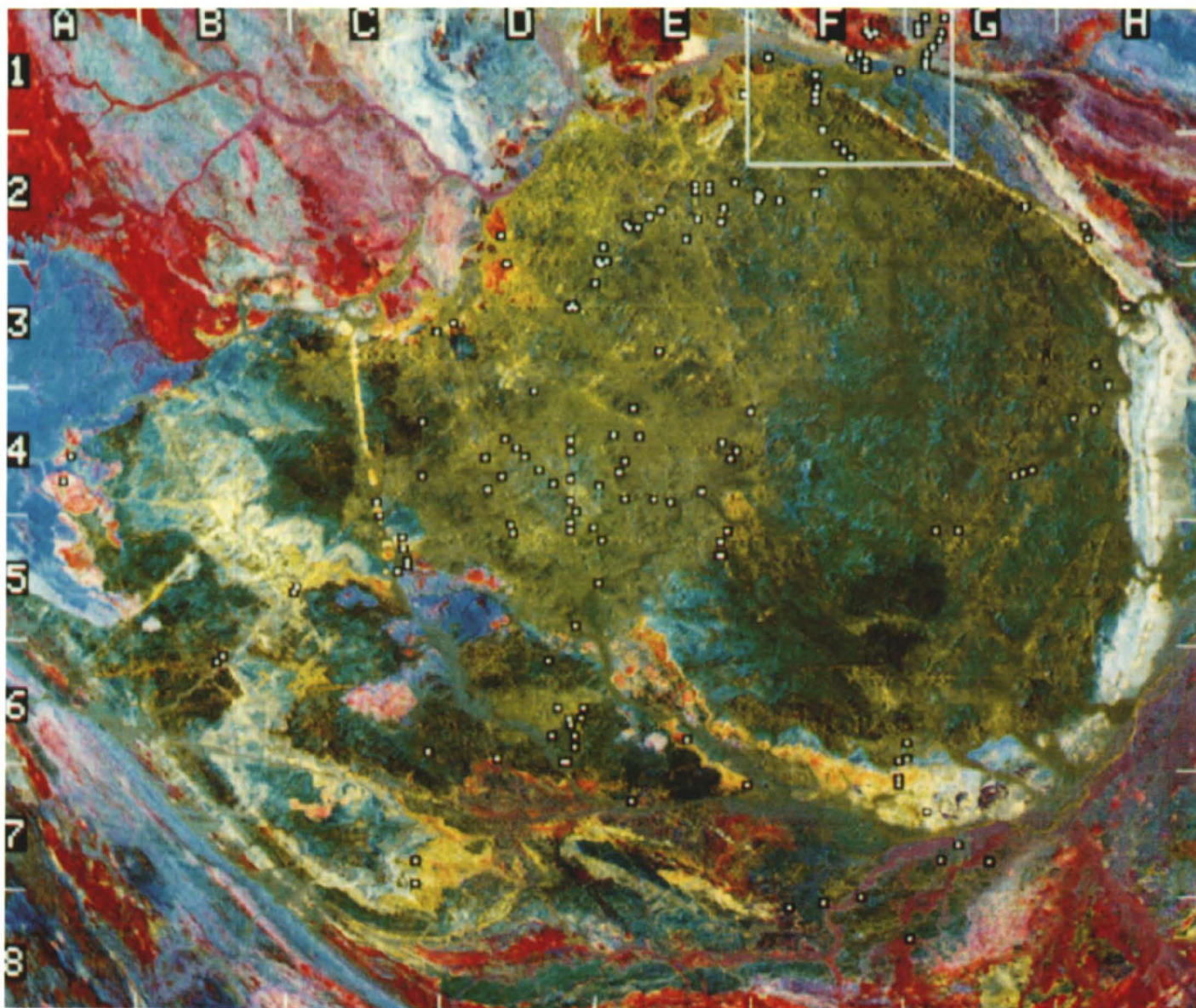


Figure 12. Color composite of TM band-5/1, band-5/7, and band-5/4 \times 3/4 ratio images for the area covered in Figure 2. Area outlined by box has been extensively sampled and is shown enlarged in Figure 13. Sample locations and tick marks are shown for reference.

band-5/7 image, the red component; and the band-5/4 \times 3/4 image, the blue component. Table 3 provides a means of predicting the colors on the composite based on the mineralogical controls for each of the ratio images discussed in previous sections. For example, serpentinites have a high abundance of hydroxyl-bearing and opaque phases, and are deficient in Fe-bearing aluminosilicates. Thus, serpentinites will be red (high band-5/7). Mafic mylonites have an abundance of hydroxyl-bearing phases and Fe-bearing aluminosilicates, but they are deficient in opaque phases. Because they have high band-5/7, band-5/4 \times 3/4, and band-5/1 values (see Fig. 11), mafic mylonites will be white in the color composite. Similarly, quartz phyllonite has an abundance of hydroxyl-

bearing phases, but is deficient in opaque phases and Fe-bearing aluminosilicates. On the color composite, therefore, the quartz phyllonite will be yellow. Granitic rocks (granite gneiss, coarse- and fine-grained granite, and tonalite) are deficient in opaques, hydroxyl-bearing phases, and Fe-bearing aluminosilicates and will have a green color in the composite. As variations in ratio data for granitic rocks are relatively small, little color variation is expected in the color composite. Unlike the other granitic rocks, quartzofeldspathic mylonite has a relatively high content of opaque phases and thus will be dark green.

The area outlined by a box in Figure 12 has been extensively sampled. An enlarged composite covering that area, together with traverse

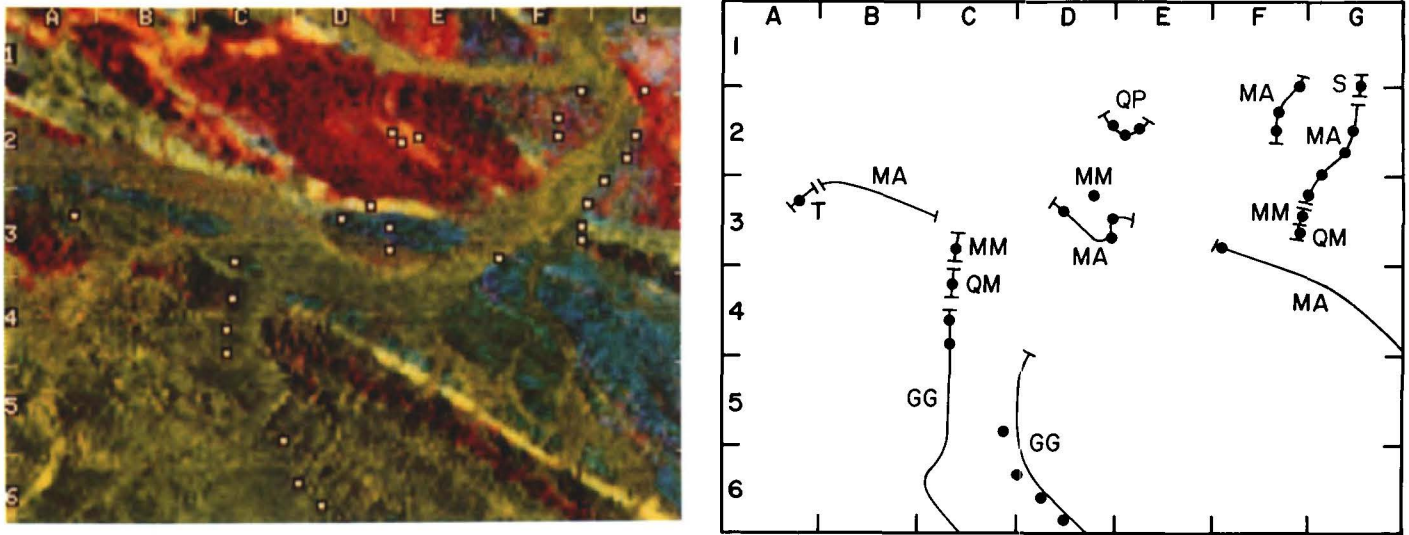


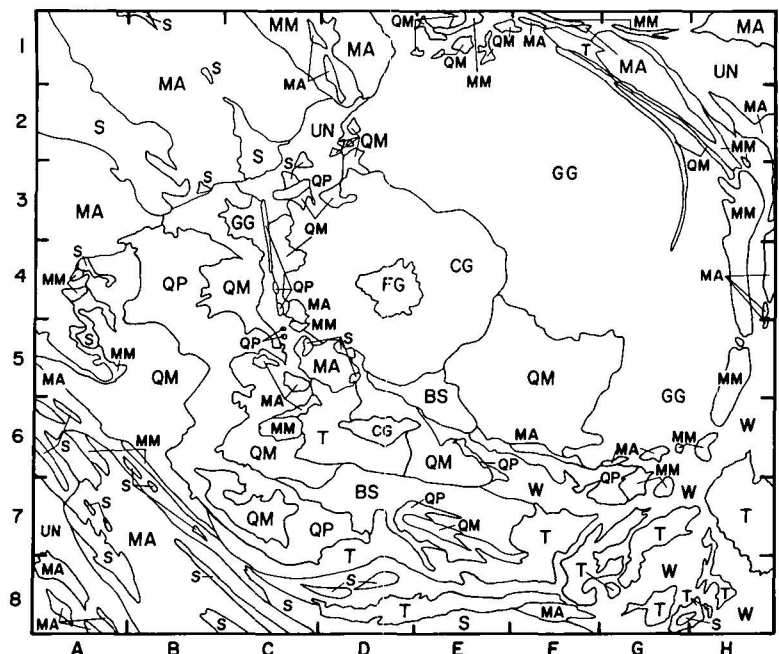
Figure 13. Left: enlargement of the area outlined by a box in Figure 12. Right: map showing rock types and sample locations along field traverses. Rock abbreviations are given in Figure 9.

and sample data, is shown in Figure 13. Once again, there is good correspondence between the colors in the enlarged composite and data presented in the traverse and sample map.

The sediments in the wadis consist primarily of mechanically weathered rock fragments that were transported downslope by flash floods, gravity, or winds. Where the sediments are compositionally similar to the adjacent mountains, the wadis become spectrally indistinguishable from their surrounding on the color composite. For example, the bright wadis in the coarse-grained granite pluton seen in Figure 8 in section D3 are

suppressed in the color composite. On the other hand, where the source rock of the sediments in the wadis is compositionally different from the adjacent mountains, the wadis maintain the spectral characteristics of their source rock and are thus spectrally distinguishable from their surroundings. For example, red wadis drain from the red serpentinite outcrop at the upper left of Figure 12 into the surrounding blue massive amphibolite outcrops. These observations confirm that the TM-based mineralogic inferences used for mapping crystalline rocks can also be successfully applied to mapping sediments in the Meatiq area.

Figure 14. Detailed lithologic map constructed from TM data for the same area shown in Figure 2. All rock abbreviations are given in Figure 9 except for UN, which refers to fine-scale undifferentiated massive amphibolite-mafic mylonite-serpentinite-biotite schist, and W, which refers to wadi sediments of diverse sources. The identification of major structural elements such as faults and folds is beyond the scope of this paper and thus these features were left off the final lithologic map. Tick marks are added for reference.



CONSTRUCTION OF A LITHOLOGIC MAP USING TM-BAND RATIO DATA

A new, detailed lithologic map for the Meatiq area was constructed (Fig. 14), using the color composite image as a mapping base. Individual band ratio images were also used. Knowledge of the general locations of rock units was critical in mapping rock units with ratios that overlap considerably on the three scatter plots. Coarse- and fine-grained granites, granite gneiss, and tonalite that have similar band ratios were therefore subdivided into finer subdivisions only where field observations are available.

In generating the new map, it was assumed that all major rock types in the Meatiq area have been sampled. In fact, no TM ratio data were found that could not be explained visually as an outcrop of one of the 10 major rock types or as an outcrop consisting of a mixture of major rock types. The presence of unidentified rock types that have ratio values that fall within the limits of the ratio values for the major rock types cannot be precluded, however. If such rocks exist, they cannot be volumetrically important because field traverse and sample data are extensive (for example, see Fig. 10D).

Mixtures of rock types occur at a variety of scales. Where the mixing units cover an image element or more, mapping was accomplished by assigning these regions to units whose predicted colors on the composite dominate the local surrounding image elements. For example, regions B-1 and B-2 are reddish-blue in the color composite, indicating a mix of serpentinite (red) and massive amphibolite (blue). Assignment of units in this area was done on the basis of the dominant color. On the basis of field observations, fine-scale interlayering of lithologic units also occurs on a single image element scale. Assignment of units in these cases was also done on the basis of the dominant color. The occasional picture elements with significantly different colors from the surrounding elements, probably due to fine-scale mixing, were ignored and were included in the rock type dominating the local region. The wadis were ignored and were included in the rock type dominating the local region, except for the wide wadis with a complex mixture of debris of diverse sources located in the lower right of Figure 14.

The most striking contrast between the TM-based lithologic map and the lithologic information contained in the earlier map (Fig. 2) is the order of magnitude increase in detail shown in the TM-based lithologic map. For example, the area previously mapped as undifferentiated "mylonitic units" can be resolved into four distinct lithologic units: quartzofeldspathic mylonite, mafic mylonite, quartz phyllonite, and biotite schist. There is good correspondence between the two maps. Minor discrepancies in lithologic boundaries between the two maps are probably due to extrapolations made in the original map where the rugged nature of the terrane rendered mapping inaccessible outcrops difficult.

SUMMARY AND IMPLICATIONS

1. Digital TM data covering the visible and reflected infrared were evaluated in terms of capabilities and limitations for lithologic mapping, using the Meatiq dome area in the hyper-arid Eastern Desert of Egypt as a test site. With ~300 km of ground traverses and 200 sample collection localities within the 30 km by 30 km test area, the Meatiq area provides rigorous ground control for many of the common major lithologies exposed in the Arabian-Nubian Shield. Bi-directional spectral reflectance (0.4–2.5 μm) data for powders of fresh samples for each of the major rock types exposed in the test area were used to guide in the selection of

TM-band reflectance ratios that maximize discrimination of individual rock types on the basis of their respective mineralogies. The ratios also suppress spectral variations within one rock type outcrop due to topography and absolute brightness. Natural rock surfaces in the test area are typically covered by a thin ($\leq 5 \mu\text{m}$), discontinuous desert varnish that consists of amorphous to poorly crystalline dioctahedral smectite, iron oxides and/or oxyhydroxides, and that has a bulk composition independent of the underlying rock type. TM data over homogeneous outcrops and bi-directional spectra for natural rock surfaces suggest that the ubiquitous varnish modulates, but does not obscure, the spectral reflectance of the underlying rocks. Comparison of ratioed TM data with field and petrographic observations shows the following trends: (a) increasing amounts of magnetite and other opaque minerals, with their low, flat spectral reflectances, decrease the ratio of TM band 5 (1.55 to 1.75) to band 1 (0.45 to 0.52 μm); (b) increasing amounts of hydroxyl-bearing minerals, with hydroxyl-related vibrational absorptions in TM band-7 wavelength region (2.08 to 2.35 μm), increase the ratio of TM band 5 to band 7; and (c) increasing amounts of Fe-bearing aluminosilicates that absorb in the band-4 wavelength region (0.76 to 0.9 μm) increase the product of the following two TM ratios: band 5 to band 4 and band 3 (0.63 to 0.69 μm) to band 4.

2. A new, detailed lithologic map was constructed for the dome area, using a color composite image generated from the three TM band ratio images. The color composite, used in combination with field and petrographic observations, shows that serpentinites can be reliably mapped on the basis of their high content of magnetite, high content of hydroxyl-bearing phases, and the lack of Fe-bearing aluminosilicates. Mafic rocks (massive amphibolite and mafic mylonite) can be distinguished from other rock types largely on the basis of the high content of Fe-bearing aluminosilicates. Coarse- and fine-grained granites, granite gneiss, and tonalite can be mapped only as a group because variations in opaque, hydroxyl-bearing, and Fe-bearing aluminosilicate phases are too small to permit separations from the ratioed TM data. Finer subdivisions were possible where detailed field traverses provide local verification. The other felsic and intermediate units, namely quartzofeldspathic mylonite, quartz phyllonite, and biotite schist, can be mapped on the basis of their relatively high content of hydroxyl-bearing phases and/or opaque phases.

3. Aerial photographs traditionally used by many field geologists as base maps provide important structural and textural information but only limited and mostly indirect information on lithology. The TM-based lithologic maps presented in this paper provide valuable mineralogic inferences that can be used for detailed mapping purposes if information regarding field relations and petrographic characteristics of rocks is also available. They are extremely valuable for mapping inaccessible complex arid terrains. Implications for mapping spectrally distinct rock types such as serpentinites, mafic, intermediate, and felsic rock units over the less well known parts of arid continents are clear.

4. Results also demonstrate both the need for, and the potential of, using systems designed to critically sample the narrowest mineral absorption features, significantly augmenting the ability to identify mineral assemblages and to map lithologic units. A Shuttle Imaging Spectrometer experiment (SISEX), with as many as 256 channels and with 10 nm passbands in the TM wavelength interval, is planned for the next decade; this will be followed by more sophisticated imaging spectrometers on the polar platforms associated with the space station (Arvidson and others, 1985; Goetz and others, 1985). When combined with deployment of similar systems in the thermal infrared (Kahle and Goetz, 1983), these new data sets will significantly augment the tools available to the field geologist for lithologic mapping.

ACKNOWLEDGMENTS

This work was supported by NASA Geology Program under Contract NASW 4017 to Washington University. We thank J. Allen, R. Batiza, B. Rivard, S. Bowring, P. Christensen, R. Couture, T. Dixon, P. Francis, G. Green, J. Luhr, W. McKinnon, R. Stern, and C. Wood for helpful comments and conversations. C. Pieters and S. Pratt kindly ran our samples through the RELAB system. S. Slavney assisted in implementing the data reduction and mapping procedures, D. Lindstrom and D. Kremser assisted in sample preparation and microprobe analyses, and B. Tani performed X-ray diffraction analyses. The images and text were prepared at the Earth and Planetary Remote Sensing Laboratory, McDonnell Center for the Space Sciences, Washington University with help from C. Martin and C. Volland.

REFERENCES CITED

- Abrams, M. J., Ashley, R. P., Rowan, L. C., Goetz, A.F.H., and Kahle, A. B., 1977, Mapping of hydrothermal alteration in the cuprite mining district, Nevada, using aircraft scanner images for the spectral region 0.46 to 2.36 μm : *Geology*, v. 5, p. 713-718.
- Adams, J. B., 1975, Interpretation of visible and near-infrared diffuse reflectance spectra of pyroxenes and other rock-forming minerals, in Karr, C. J., ed., *Infrared and raman spectroscopy of lunar and terrestrial minerals*: New York, Academic Press, p. 91-116.
- Adams, J. B., and Filice, A. L., 1967, Spectral reflectance 0.4 to 2.0 microns of silicate rock powders: *Journal of Geophysical Research*, v. 72, p. 5705-5715.
- Adams, J. B., and others, 1982, Interpretation of weathered surfaces in arid regions using Landsat multispectral images: Thematic Conference: Remote sensing of arid and semi-arid lands: Cairo, Egypt.
- Allen, C. C., 1978, Desert varnish of the Sonoran Desert—Optical and electron probe microanalysis: *Journal of Geology*, v. 86, p. 743-752.
- Arvidson, R. E., Buther, D. M., and Hartle, R. E., 1985, Eos: The Earth observing system of the 1990s, in *Institute of Electrical and Electronics Engineers, Proceedings, Special issue on perceiving Earth's resources from space*: New York, v. 73, p. 1025-1030.
- Baird, A. K., 1984a, Granitic terrains viewed remotely by shuttle infra-red radiometry: Some compositional predictions: *Journal of Geophysical Research*, v. 89, p. 9439-9447.
- 1984b, Rapid discrimination of granitic rock compositions by low-resolution near-infrared reflectance: *Journal of Geophysical Research*, v. 89, p. 2491-2496.
- 1984c, Iron variation within a granitic pluton as determined by near-infrared reflectance: *Journal of Geology*, v. 92, p. 344-351.
- Barker, J. L., Ball, D. L., Lung, K. C., and Walker, J. A., 1985, Prelaunch absolute radiometric calibration of the reflective bands on the Landsat-4 Protoflight Thematic Mapper, in *Landsat-4 Early Results Symposium, Proceedings: NASA Conference Publication 2355, v. II, Thematic Mapper (TM), Part 1*, p. 277-372.
- Blom, R. G., Abrams, M. J., and Adams, H. G., 1980, Spectral reflectance and discrimination of plutonic rocks in the 0.45- to 2.45- μm region: *Journal of Geophysical Research*, v. 85, p. 2638-2648.
- Engel, C. G., and Sharp, R. P., 1958, Chemical data on desert varnish: *Geological Society of America Bulletin*, v. 69, p. 487-518.
- Engel, J. L., and Weinstein, O., 1982, The Thematic Mapper—An overview, in *International Geoscience and Remote Sensing Symposium, Munich, 1982, Digest: Institute of Electrical and Electronics Engineers*, v. 1, p. WP1.1-1.7.
- Goetz, A.F.H., Wellman, J. E., and Barnes, W. L., 1985, Optical remote sensing of the Earth, in *Institute of Electrical and Electronics Engineers, Proceedings, Special issue on perceiving Earth's resources from space*: New York, v. 73, p. 950-969.
- Gradie, J., Veverka, J., and Ituratti, B., 1980, The effects of scattering geometry on the spectrophotometric properties of powdered materials, in *Lunar and Planetary Science Conference, 11th, Proceedings*, p. 799-815.
- Guinness, E. A., Arvidson, R. E., Dale-Bannister, M. A., Singer, R. B., and Bruckenthal, E. A., 1987, On the spectral reflectance properties of materials exposed at the Viking landing sites: *Journal of Geophysical Research*, v. 92, p. E575-E587.
- Hunt, G. R., 1977, Spectral signatures of particulate minerals in the visible and near-infrared: *Geophysics*, v. 42, p. 501-513.
- Hunt, G. R., and Salisbury, J. W., 1970, Visible and near-infrared spectra of minerals and rocks: I. Silicate minerals: *Modern Geology*, v. 1, p. 283-300.
- 1971, Visible and near-infrared spectra of minerals and rocks: II. Carbonates: *Modern Geology*, v. 2, p. 23-30.
- Hunt, G. R., Salisbury, J. W., and Lenhoff, C. J., 1971, Visible and near-infrared spectra of minerals and rocks: III. Oxides and hydroxides: *Modern Geology*, v. 2, p. 195-205.
- 1973a, Visible and near-infrared spectra of minerals and rocks: VI. Additional silicates: *Modern Geology*, v. 4, p. 85-106.
- 1973b, Visible and near-infrared spectra of minerals and rocks: VIII. Intermediate igneous rocks: *Modern Geology*, v. 4, p. 237-244.
- 1973c, Visible and near-infrared spectra of minerals and rocks: VII. Acidic igneous rocks: *Modern Geology*, v. 4, p. 217-224.
- 1974, Visible and near-infrared spectra of minerals and rocks: IX. Basic and ultrabasic igneous rocks: *Modern Geology*, v. 5, p. 15-22.
- Jeffery, P. G., 1975, *Chemical methods of rock analysis* (2nd edition): Oxford, England, Pergamon Press, 525 p.
- Kailath, T., 1967, The divergence and Bhattacharyya distance measures in signal selection: *Institute of Electrical and Electronics Engineers, Transactions in Communication Technology*, v. 15, no. 1, p. 52-60.
- Kahle, A. B., and others, 1983, Mineralogical information from a new airborne thermal infrared multispectral scanner: *Science*, v. 222, p. 24-27.
- Maxwell, J. A., 1968, *Rock and mineral analysis*: New York, Interscience Publishers, 584 p.
- Norrish, K., and Hutton, J. T., 1969, An accurate X-ray spectrographic method for the analysis of a wide range of geological samples: *Geochimica et Cosmochimica Acta*, v. 33, p. 431-454.
- Pieters, C. M., 1983, Strength of mineral absorption features in the transmitted component of near-infrared reflected light: First results from RELAB: *Journal of Geophysical Research*, v. 88, p. 9534-9544.
- Potter, R. M., and Rossman, G. R., 1977, Desert varnish: The importance of clay minerals: *Science*, v. 196, p. 1446-1448.
- 1979, The manganese- and iron-oxide mineralogy of desert varnish: *Chemical Geology*, v. 25, p. 79-94.
- Rowan, L. C., Wetlaufer, P. W., Goetz, A.F.H., Billingsley, F. C., and Stewart, J. H., 1975, Discrimination of rock types and detection of hydrothermally altered areas in south-central Nevada by use of computer-enhanced ERTS images: *U.S. Geological Survey Professional Paper 883*, 35 p.
- Shackleton, R. M., Ries, A. C., Graham, R. H., and Fitches, W. R., 1980, Late Precambrian ophiolitic melange in the eastern desert of Egypt: *Nature*, v. 285, p. 472-474.
- Singer, R. B., 1981, Near-infrared spectral reflectance of mineral mixtures: Systematic combinations of pyroxenes, olivines, and iron oxides: *Journal of Geophysical Research*, v. 86, p. 7967-7982.
- Sturchio, N. C., 1983, *Geology, petrology, and geochronology of the metamorphic rocks of Meatiq Dome, central Eastern Desert, Egypt* [Ph.D. thesis]: St. Louis, Missouri, Washington University, 218 p.
- Sturchio, N. C., and Muehlenbachs, K., 1985, Origin of low- ^{18}O metamorphic rocks from a late Proterozoic shear zone in the Eastern Desert of Egypt: *Contributions to Mineralogy and Petrology*, v. 91, p. 188-195.
- Sturchio, N. C., Sultan, M., and Batiza, R., 1983, Geology and origin of the Meatiq Dome, Egypt: A Precambrian metamorphic core complex? *Geology*, v. 11, p. 72-76.
- Sturchio, N. C., Sultan, M., Batiza, R., Hedge, C., El Shazly, E. M., and Abdel-Maguid, A., 1984, Geology, age and origin of the Meatiq Dome: Implications for the Precambrian stratigraphy and tectonic evolution of the Eastern Desert of Egypt, in Bakor, A. R., and others, eds., *Pan-African crustal evolution in the Arabian-Nubian Shield: Jeddah, Saudi Arabia, Bulletin of the Faculty of Earth Sciences, King Abdul Aziz University*, v. 6, p. 127-143.
- Sultan, M., 1984, *Geology, petrology, and geochemistry of a Younger Granite pluton, central Eastern Desert of Egypt: importance of mixing* [Ph.D. thesis]: St. Louis, Missouri, Washington University, 218 p.
- Sultan, M., Arvidson, R., and Sturchio, N. C., 1986a, Digital mapping of ophiolite melange zones from Landsat thematic mapper (TM) data in arid areas: Meatiq dome, Egypt: *Geological Society of America Abstracts with Programs*, v. 18, p. 766.
- 1986b, Mapping of serpentinites using Landsat thematic mapper data in the Eastern Desert of Egypt: *Geology*, v. 14, p. 995-999.
- Sultan, M., Batiza, R., and Sturchio, N. C., 1986c, The origin of small-scale geochemical and mineralogical variations in a granite intrusion: a crystallization and mixing model: *Contributions to Mineralogy and Petrology*, v. 93, p. 513-523.
- Van Der Plas, H., and Tobi, A. C., 1965, A chart for judging the reliability of point counting results: *American Journal of Science*, v. 263, p. 87-90.

MANUSCRIPT RECEIVED BY THE SOCIETY NOVEMBER 4, 1986

REVISED MANUSCRIPT RECEIVED APRIL 28, 1987

MANUSCRIPT ACCEPTED MAY 4, 1987